Science Advances
AAAS

advances.sciencemag.org/cgi/content/full/5/4/eaav4580/DC1

Supplementary Materials for

A pan-coronavirus fusion inhibitor targeting the HR1 domain of human coronavirus spike

Shuai Xia, Lei Yan, Wei Xu, Anurodh Shankar Agrawal, Abdullah Algaissi, Chien-Te K. Tseng, Qian Wang, Lanying Du, Wenjie Tan, Ian A. Wilson*, Shibo Jiang*, Bei Yang*, Lu Lu*

*Corresponding author. Email: wilson@scripps.edu (I.A.W.); shibojiang@fudan.edu.cn (S.J.); yangbei@shanghaitech.edu.cn (B.Y.); lul@fudan.edu.cn (L.L.)

Published 10 April 2019, *Sci. Adv.* **5**, eaav4580 (2019)
DOI: 10.1126/sciadv.aav4580

This PDF file includes:

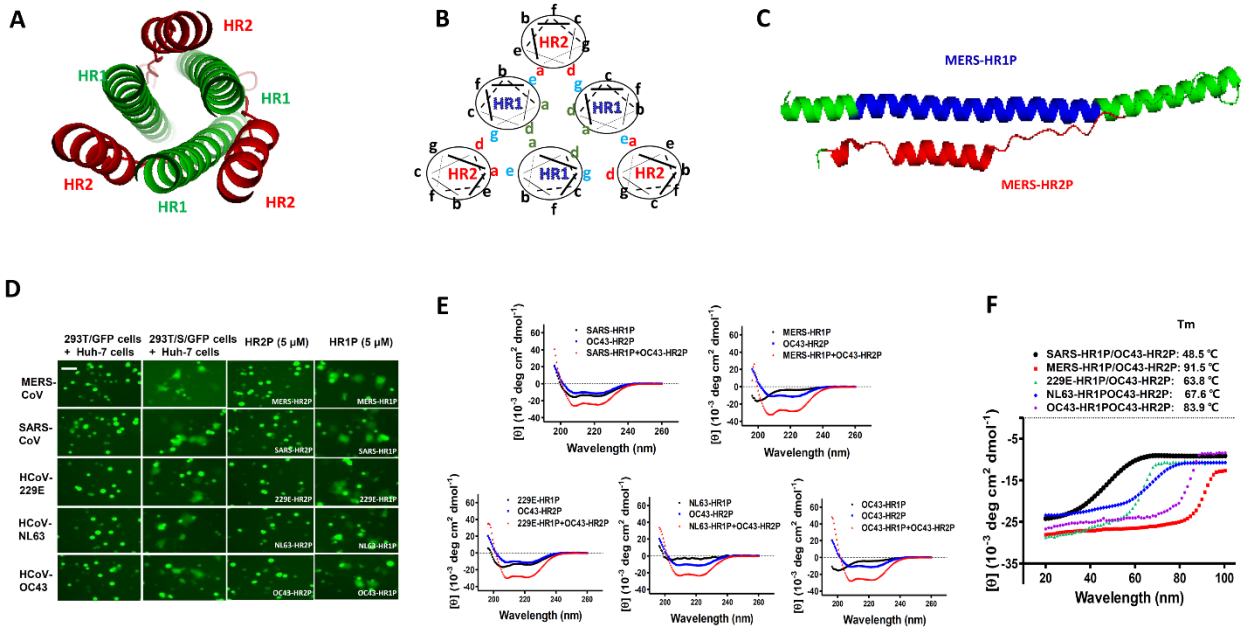

Fig. S1. Interaction between HCoV HR1 and HR2 regions in HCoV S proteins. (**A**) Cartoon of the MERS-CoV 6-HB structure, with HR1 colored in green and HR2 colored in red, respectively (PDB: 4NJL). (**B**) The three HR1s interact through residues located at the "*a*" and "*d*" positions (green) to form the triple-helix trimeric core. Residues of HR1 located at the "*e*" and "*g*" positions (blue) interact with "*a*" and "*d*" residues (red) in HR2 to form the 6-HB structure. (**C**) Structural location of MERS-HR1P (green) and MERS-HR2P (red) in MERS-CoV HR1 and HR2 (PDB: 4NJL). (**D**) Establishment of multiple cell-cell fusion assays mediated by the S protein of MERS-CoV, SARS-CoV, HCoV-229E, HCoV-NL63 and HCoV-OC43, respectively. After Huh-7 cells were co-cultured with 293T/EGFP or 293T/S/EGFP cells in the absence or presence of 5 μM of HR2P or 5 μM of HR1P at 37 °C for 2-4 h, cell–cell fusion was imaged under an optical microscope with fluorescence. Scale bar, 800 μm. (**E**) CD spectra of various HR1P/OC43-HR2P complexes in phosphate buffer. (**F**) The melting curves of various HR1P/OC43-HR2P complexes.

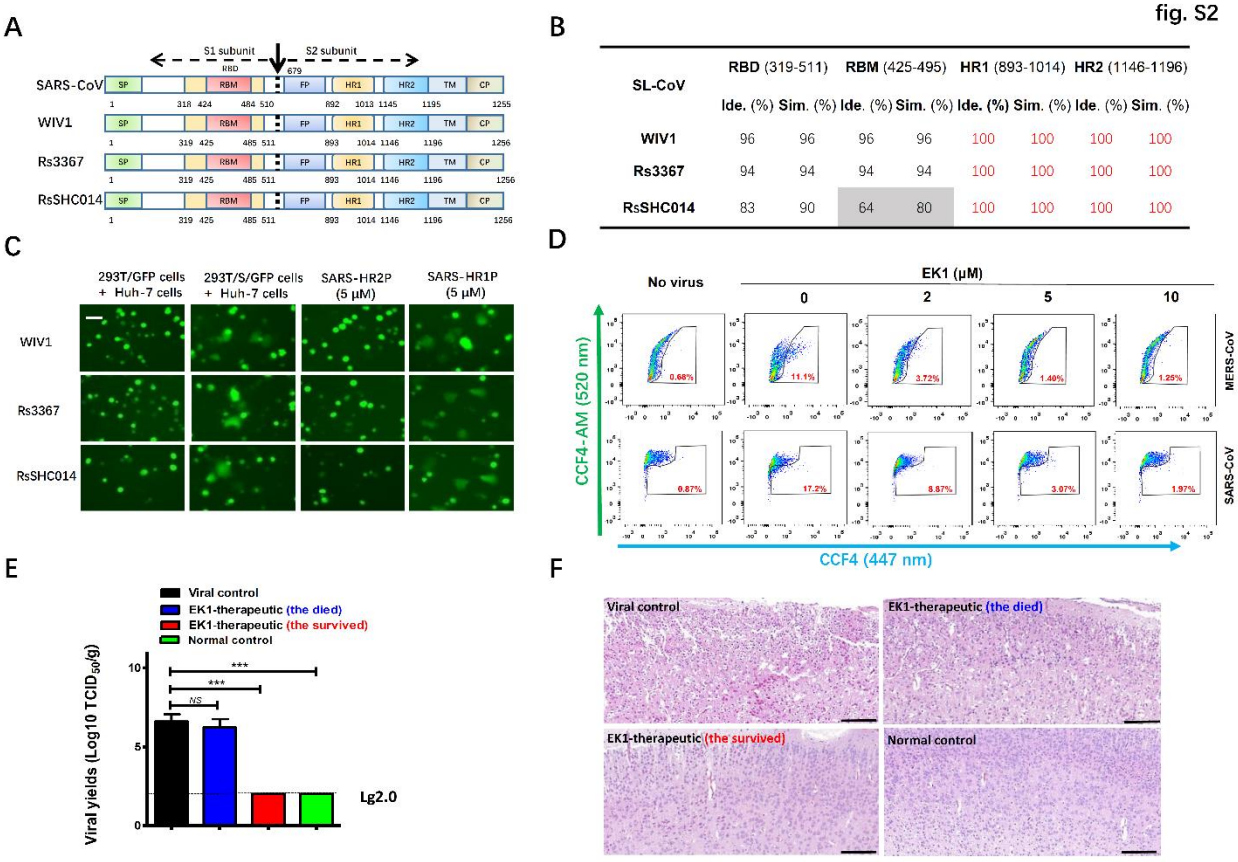

SL-CoV	RBD (319-511)		RBM (425-495)		HR1 (893-1014)		HR2 (1146-1196)	
	Ide. (%)	Sim. (%)	Ide. (%)	Sim. (%)	Ide. (%)	Sim. (%)	Ide. (%)	Sim. (%)
WIV1	96	96	96	96	100	100	100	100
Rs3367	94	94	94	94	100	100	100	100
RsSHC014	83	90	64	80	100	100	100	100

Fig. S2. Identity and similarity in spike protein sequences of SARS-CoV and SL-CoVs and the effect of EK1 on HCoV S protein–mediated cell fusion and virus-cell fusion, as well as the viral loads and histopathological changes in brains of HCoV-infected mice. (**A**) Schematic representation of S proteins of SARS-CoVs and SL-CoVs. Residue numbers correspond to their positions in S protein of SARS-CoV. (**B**) The identity and similarity of RBD, RBM, HR1 and HR2 sequences of SL-CoVs to those of SARS-CoV. (**C**) Establishment of the cell-cell fusion systems mediated by S protein of SL-CoV-W1V1, SL-CoV-Rs3367 and SL-CoV-SHC014, respectively. Huh-7 cells and 293T/S/EGFP cells (or 293T/EGFP cells) were co-cultured in the absence or presence of 5 μM of SARS-HR2P or 5 μM of SARS-HR1P at 37 °C for 4 h, and then photographed under fluorescence microscopy. Scale bar, 800 μm. (**D**) EK1 inhibits entry of MERS-CoV and SARS-CoV Blam-Vpr virions into the target cells. (**E**) The viral load of brains from the viral control mice, HCoV-OC43 infected mice that either survived or died during EK1 therapeutic treatment, and normal control mice. (**F**) Histological examination of brains from the viral control mice, HCoV-OC43 infected mice that either survived or died during EK1 therapeutic treatment, and normal control mice.

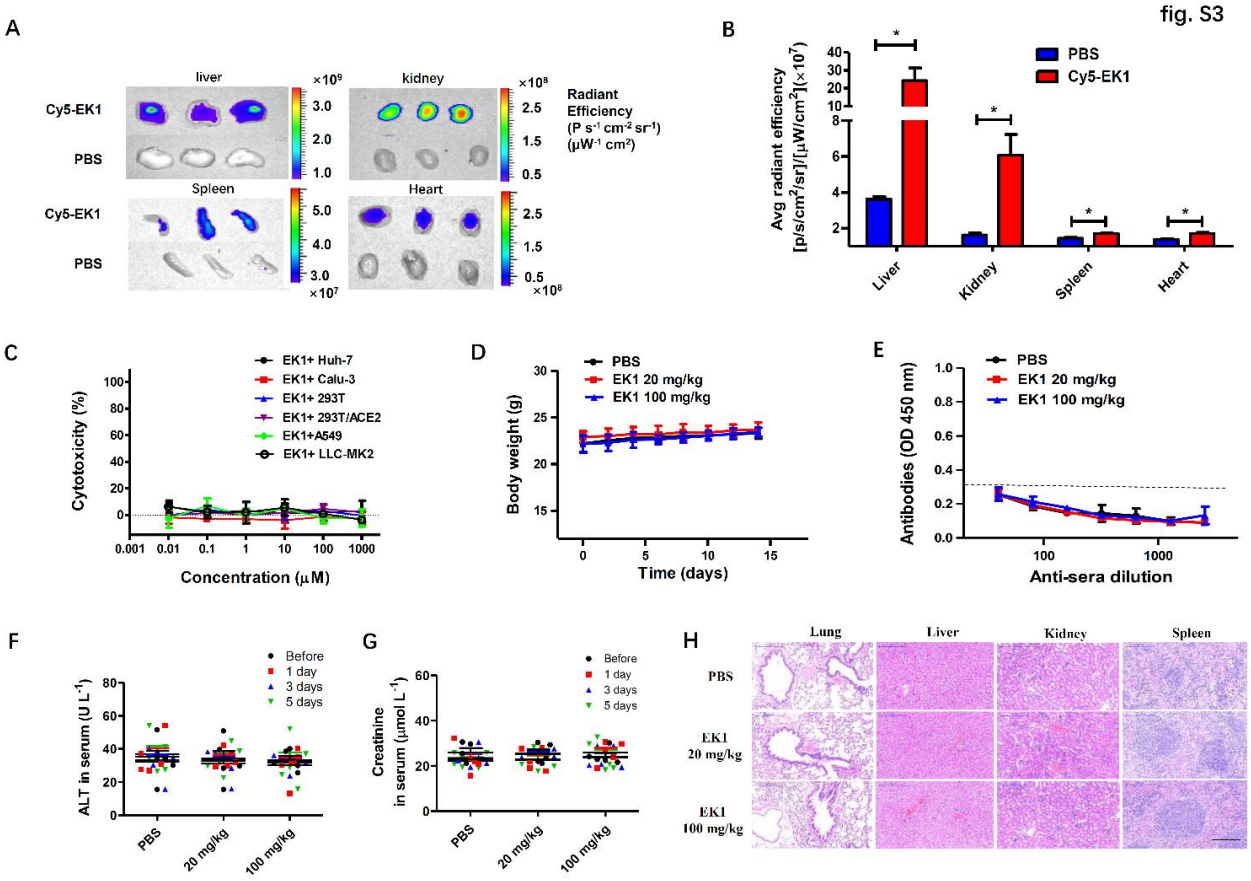

Fig. S3. In vivo safety of EK1 through intranasal administration. (**A**) Distribution of EK1 in other organs after intranasal administration. (**B**) Statistical analysis of results from B. Data are means ± s.d. *P<0.05, Student's two-tailed t-test. (**C**) Cytotoxicity of EK1 on various target cells. No cytotoxicity of EK1 was found on Huh-7, A549, LLC-MK2, Calu-3, 293T and 293T/ACE2 cells. Data are means ± s.d. of triplicate samples from a representative experiment. (**D**) Body weight change of each group of mice treated with EK1 (20 mg/kg), EK1 (100 mg/kg), or PBS was recorded up to 2 weeks post-treatment. (**E**) The titer of IgG sera to EK1 in each group of mice two weeks post-treatment. (**F**) ALT in the sera of each group of mice before the first treatment and 1, 3 and 5 days post-final treatment. All error bars reflect s.d. (**G**) Creatinine in the sera of the mice at the above time points. All error bars reflect s.d. (**H**) Comparison of hematoxylin and eosin staining of organ tissues, including lung, liver, kidney, spleen from each group of mice. Scale bar, 200 μm.

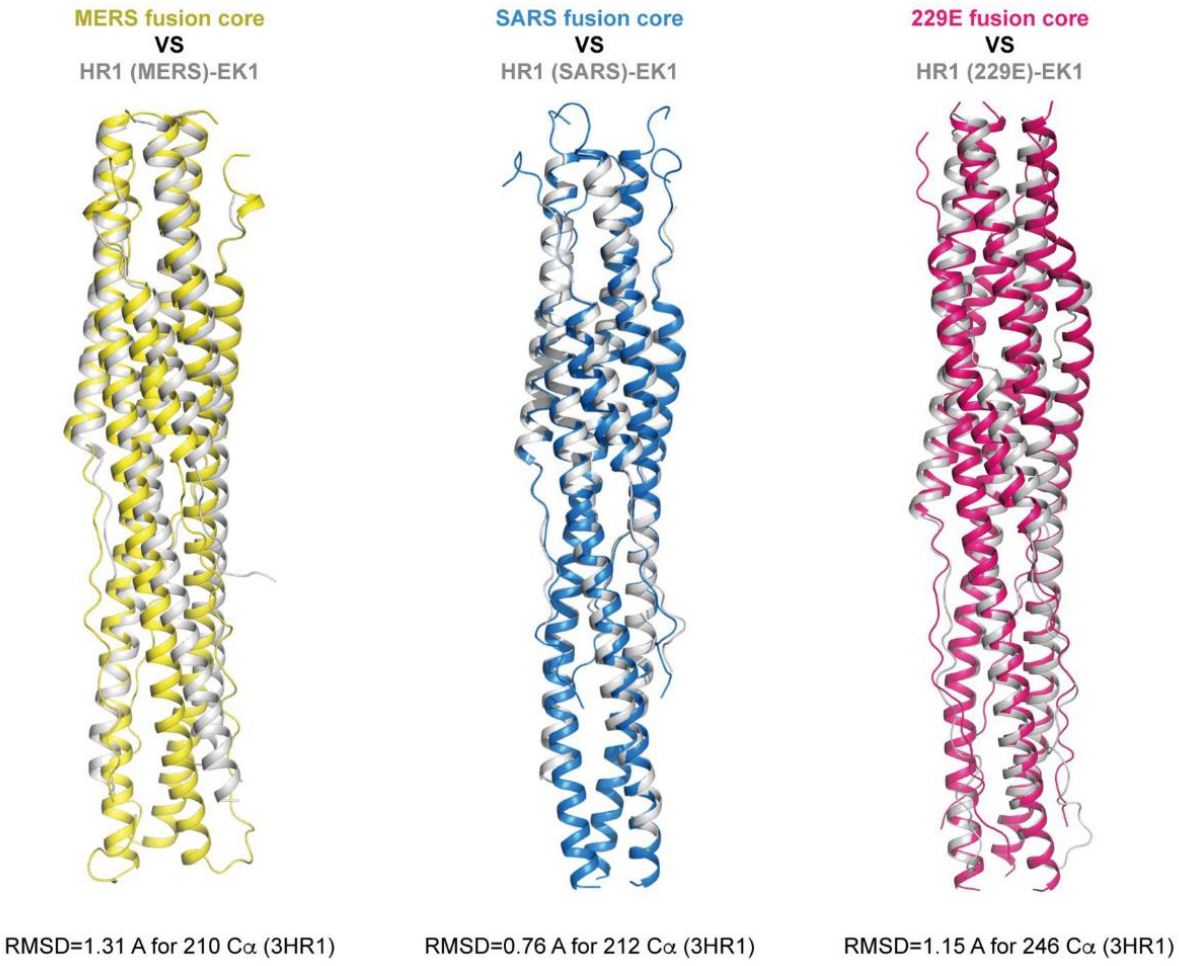

Fig. S4. Structural comparison between the HR1-EK1 6-HB bundles and cognate HR1-HR2 6-HB bundles reveals that the EK1 peptide binds to the triple-helix HR1 core of different HCoVs in a similar manner to that of the native HR2 of the corresponding HCoV. The superposition shows overlaps of EK1 and HR2 and no major conformational changes in HR1 upon EK1 binding as compared to HR2. The crystal structure of HR1(MERS)-L6-EK1 was aligned with 3HR1(MERS)-3HR2 fusion-core structures (PDBid: 4njl) with an RMSD of 1.31 Å over 210 equivalent Cα's from three HR1s. The structure of HR1(SARS)-L6-EK1 or HR1(229E)-L6-EK1was aligned with corresponding fusion-core structures (PDBid: 1wyy and 5yl9) with an RMSD of 0.76 Å over 212 equivalent Cα's and 1.15 Å over 246 equivalent Cα's , respectively.

fig.S5

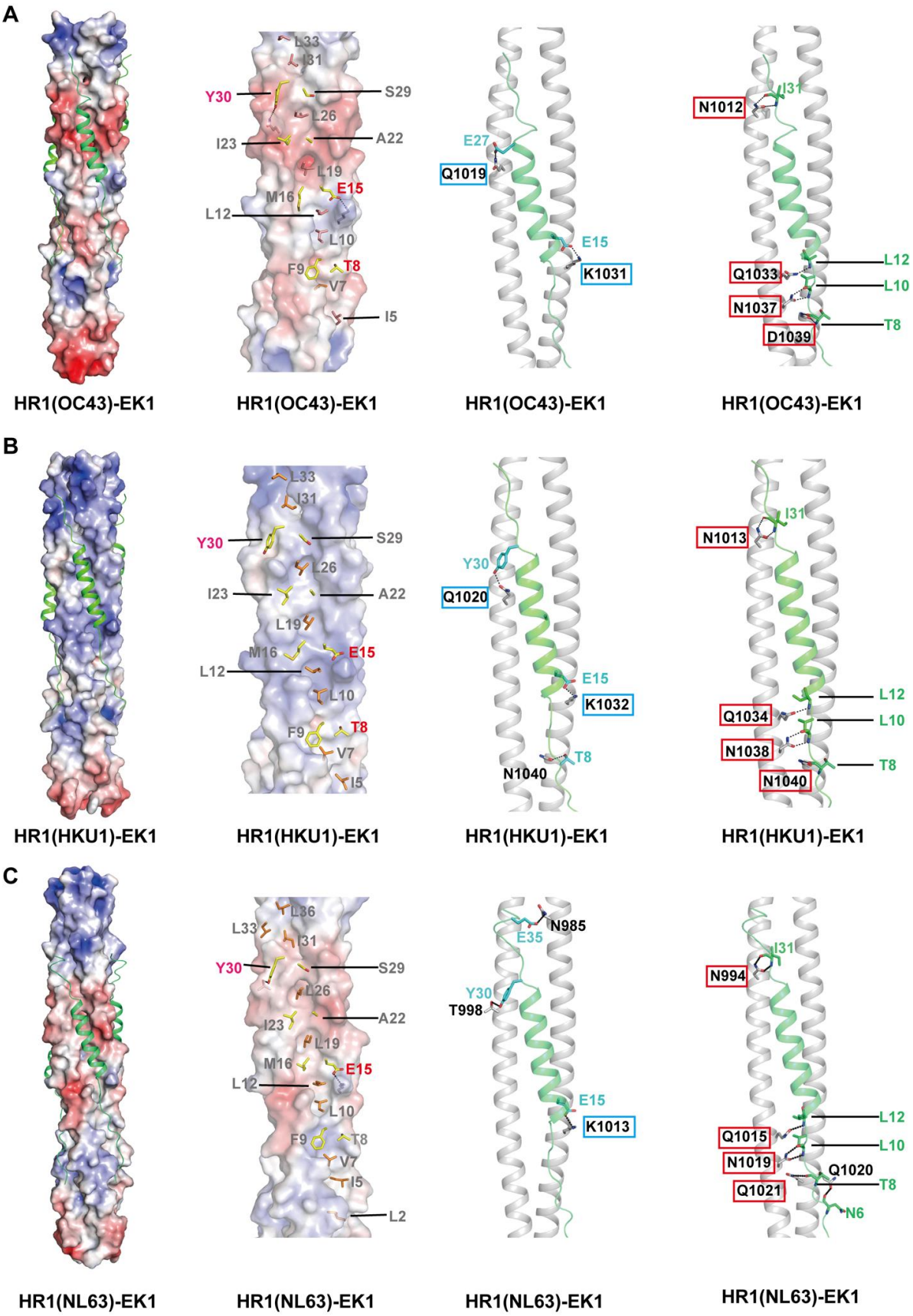
A
L33
I31
Y30
S29
L26
I23
A22
L19
E15
M16
L12
L10
F9
T8
V7
I5
E27
Q1019
E15
K1031
N1012
I31
L12
Q1033
L10
N1037
T8
D1039
HR1(OC43)-EK1
HR1(OC43)-EK1
HR1(OC43)-EK1
HR1(OC43)-EK1
B
L33
I31
Y30
S29
L26
I23
A22
L19
M16
E15
L12
L10
F9
T8
V7
I5
Y30
Q1020
E15
K1032
T8
N1040
N1013
I31
L12
Q1034
L10
N1038
T8
N1040
HR1(HKU1)-EK1
HR1(HKU1)-EK1
HR1(HKU1)-EK1
HR1(HKU1)-EK1
C
L36
L33
I31
Y30
S29
L26
I23
A22
L19
M16
E15
L12
L10
F9
T8
V7
I5
L2
E35
N985
Y30
T998
E15
K1013
N994
I31
L12
Q1015
L10
N1019
Q1020
T8
Q1021
N6
HR1(NL63)-EK1
HR1(NL63)-EK1
HR1(NL63)-EK1
HR1(NL63)-EK1

Fig. S5. The EK1 peptide forms 6-helical bundle structures with the HR1 motifs from OC43, HKU1, and NL63. (**A**-**C**) 1st panel: overall structures, of HR1-EK1 complexes, with the 3HR1 cores illustrated as electrostatic surfaces and EK1 depicted as a ribbon diagram; 2nd panel: hydrophobic packings between EK1 and corresponding triple-helix HR1 hydrophobic cores, note that the extensive hydrophobic packing between EK1 and OC43, HKU1 or NL63 3HR1 cores is conserved, when compared to that between EK1 and SARS-CoV, MERS-CoV or HCoV-229E. Residues on EK1 that are involved in hydrophobic packing are shown as stick models on the electrostatic surfaces of 3HR1 cores; 3rd panel: side-chain to side-chain hydrophilic interactions between EK1 and corresponding triple-helix HR1 cores. HR1 residues of HCoV-OC43, HCoV-HKU1 and HCoV-NL63 that meditate highly conserved side-chain to side-chain hydrophilic interactions with EK1 residues are boxed in cyan; 4th panel: main-chain to side-chain polar interactions between EK1 and corresponding triple-helix HR1 cores. The HR1 residues of HCoV-OC43, HCoV-HKU1 and HCoV-NL63 that meditate highly conserved side-chain to main-chain hydrophilic interactions with EK1 residues are boxed in red.

fig.S6

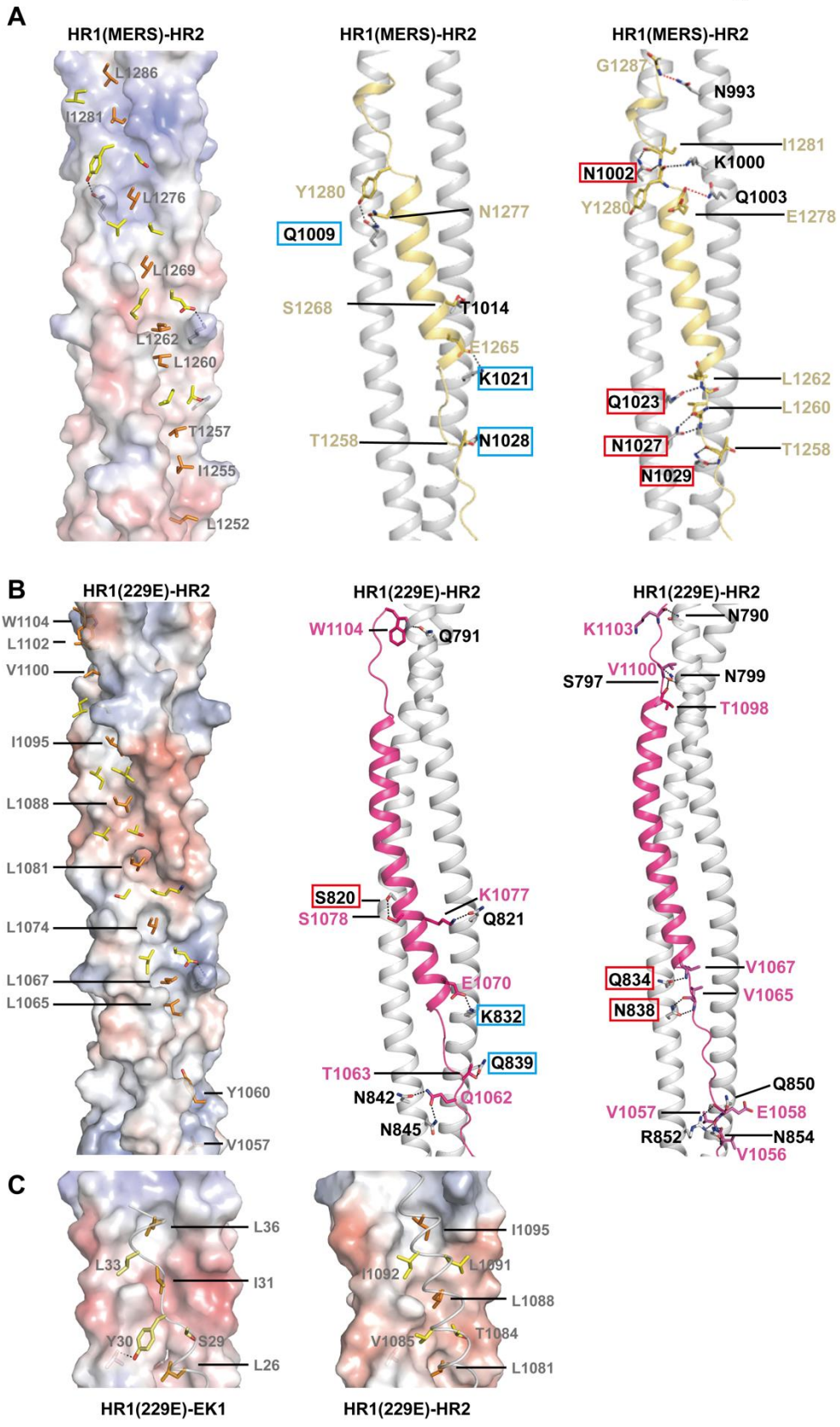
A
HR1(MERS)-HR2
L1286
I1281
L1276
L1269
L1262
L1260
T1257
I1255
L1252
HR1(MERS)-HR2
Y1280
N1277
Q1009
S1268
T1014
E1265
K1021
T1258
N1028
HR1(MERS)-HR2
G1287
N993
I1281
K1000
N1002
Q1003
Y1280
E1278
L1262
Q1023
L1260
N1027
T1258
N1029
B
HR1(229E)-HR2
W1104
L1102
V1100
I1095
L1088
L1081
L1074
L1067
L1065
Y1060
V1057
HR1(229E)-HR2
W1104
Q791
S820
K1077
S1078
Q821
E1070
K832
Q839
T1063
N842
Q1062
N845
HR1(229E)-HR2
K1103
N790
V1100
S797
N799
T1098
Q834
V1067
V1065
N838
Q850
V1057
E1058
R852
N854
V1056
C
L36
L33
I31
Y30
S29
L26
HR1(229E)-EK1
I1095
I1092
L1091
L1088
T1084
V1085
L1081
HR1(229E)-HR2

Fig. S6. Interactions between the HR1 and HR2 motifs of MERS and 229E. Hydrophobic interactions (left panel), side-chain to side-chain hydrophilic interactions (middle panel) and side-chain to main-chain polar interactions (right panel) between the HR1 and HR2 motifs of MERS-CoV (**A**) and HCoV-229E (**B**). (A-B) Left panel: HR2 residues that are involved in hydrophobic packing are shown as stick models on the electrostatic surfaces of 3HR1 cores. For clarity, only 'burying residues' are labeled in grey. Middle and right panel: HR1 residues that are highlighted in cyan (middle panel) and red (right panel) boxes are the same residues that meditate conserved side-chain to side-chain and side-chain to main-chain hydrophilic interactions with EK1 residues. (**C**) Close-up view of the C-terminal extended region of EK1 in the HR1(229E)-EK1 structure (left) and its equivalent region in the HR1(229E)-HR2 structure (right).

fig. S7

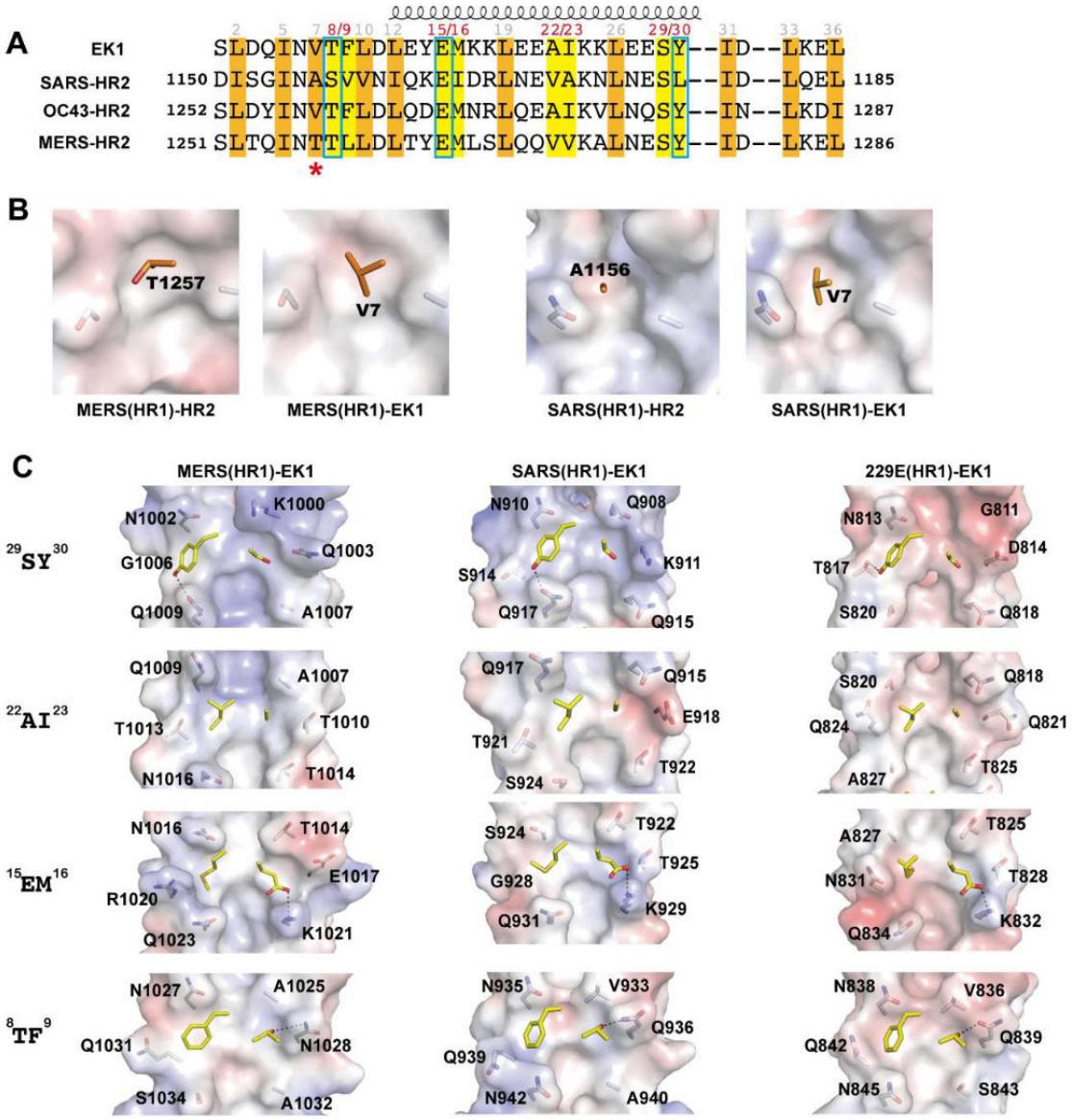

Fig. S7. Key residues at critical positions endow EK1 and OC43-HR2 with pan-CoV activity. (**A**) Schematic representation illustrating the similarity and variation of the burying and packing residues across different α-HCoVs. (**B**) V7EK1 outcompetes native T1257MERS and A1156SARS at corresponding position for fitting onto HR1. (**C**) Surface representation illustrating how ridge-packing residues from EK1 can accommodate the different shapes and electrostatic potential of ridges from different HCoVs.

Table S1. Inhibitory activity of peptides on multiple cell-cell fusion assays.

Cell-cell fusion assays	Inhibitory activity of peptides, IC_{50} (μM)											
	SARS-CoV		MERS-CoV		HCoV-229E		HCoV-NL63		HCoV-OC43		EK1	Scrambled
	HR1P	HR2P	HR1P	HR2P	HR1P	HR2P	HR1P	HR2P	HR1P	HR2P		
SARS-CoV	>5.00	0.52±0.11	>5.00	>5.00	>5.00	>5.00	>5.00	>5.00	>5.00	0.54±0.11	0.27±0.01	>5.00
MERS-CoV	>5.00	>5.00	>5.00	1.01±0.13	>5.00	>5.00	>5.00	>5.00	>5.00	0.39±0.08	0.18±0.01	>5.00
HCoV-229E	>5.00	>5.00	>5.00	>5.00	>5.00	0.13±0.02	>5.00	0.56±0.09	>5.00	0.84±0.19	0.15±0.01	>5.00
HCoV-NL63	>5.00	>5.00	>5.00	>5.00	>5.00	0.51±0.06	>5.00	0.21±0.02	>5.00	0.94±0.11	0.63±0.18	>5.00
HCoV-OC43	>5.00	>5.00	>5.00	>5.00	>5.00	>5.00	>5.00	>5.00	>5.00	0.66±0.16	0.33±0.05	>5.00

IC_{50}: Concentration of peptide at which 50% of HCoV S-mediated cell–cell fusion is blocked. Values greater than 5 μM are in a gray background; 1-5 μM in a green background; 0.5-1 μM in an orange background; and less than 0.5 μM in a red background.

Table S2. Solubility and fusion inhibitory activities of different peptides.

Peptide	Sequence	Solubility (μM) in		IC_{50} of cell-cell fusion (μM)				
		PBS (pH=7.2)	Water	MERS-CoV	SARS-CoV	HCoV-229E	HCoV-NL63	HCoV-OC43
OC43-HR2P	SLDYINVTFLDLQDEMNRLQEAIKVLNQSYINLKDI	445±7	44±5	0.36±0.07	0.54±0.07	0.93±0.04	0.99±0.14	0.52±0.10
EK0-1	SLDYINVTFLDLQDEM***KK***L***E***EAIK***K***L***E***QSYINLKDI	219±14	9511±272	0.32±0.03	0.31±0.03	0.30±0.05	0.78±0.10	0.42±0.04
EK0-2	SLDYINVTFLDL***E***DEM***KK***L***E***EAIK***K***L***EE***SYINLK***E***I	528±19	10683±454	0.26±0.02	0.25±0.02	0.22±0.05	0.63±0.12	0.53±0.15
EK0-3	SLD***Q***INVTFLDL***EY***EM***KK***L***E***EAIK***K***L***EE***SYI***D***LK***E***I	1083±83	19421±238	0.22±0.04	0.25±0.02	0.32±0.03	0.78±0.18	0.49±0.11
EK1	SLD***Q***INVTFLDL***EY***EM***KK***L***E***EAIK***K***L***EE***SYI***D***LK***EL***	1542±115	20953±1154	0.19±0.01	0.21±0.01	0.20±0.05	0.62±0.17	0.39±0.04

IC_{50}: Concentration of peptide at which 50% of HCoV S-mediated cell–cell fusion was blocked.

*The introduced Glu (E), Lys (K) and other residues are highlighted in red, bold and italics.

Table S3. Data collection and structural refinement statistics.

	HR1(MERS)-EK1	HR1(SARS)-EK1	HR1(229E)-EK1
Data collection statistics			
Resolution range (Å)*	25.8-3.31 (3.43-3.31)	34.5-3.30(3.42-3.30)	44.4- 2.21 (2.29-2.21)
Space group	$P3_121$	$P4_32_12$	C121
Unit cell (Å,°)	60.3 60.3 175.2	101.0 101.0 73.4	95.6 45.6 94.8
	90 90 120	90 90 90	90 96.3 90
Unique reflections*	5955 (564)	6070 (595)	20,441 (1954)
Redundancy*	11.7 (11.8)	8.1 (7.8)	4.7 (4.5)
Completeness (%)*	99.9 (100)	99.9 (100)	99.4 (99.5)
Mean I/s*	20.7 (2.5)	11.9 (1.5)	18.9 (5.0)
Wilson B ($Å^2$)	109	98	26
R_{meas} (%)*, [a]	12.2 (77.5)	17.2 (102.4)	8.7 (21.7)
R_{pim} (%)*, [b]	3.6 (32.4)	6.0 (36.3)	4.0 (9.7)
$CC_{1/2}$*, [c]	(0.897)	(0.740)	(0.979)
Refinement statistics			
Reflections used in refinement*	5953 (564)	6060 (595)	20,374 (1952)
Reflections used for R_{free}*	339 (23)	307 (40)	1017 (106)
R_{work} (%)*, [d]	25.9 (34.0)	25.3 (31.4)	21.0 (23.0)
R_{free} (%)*, [d]	31.4 (31.8)	30.9 (34.5)	24.7 (30.4)
Protein atoms	2341	2443	2950
Solvent atoms	0	0	110
Ligand atoms	0	0	2
RMSD bond length (Å)	0.003	0.01	0.01
RMSD bond angles (°)	0.56	1.17	1.22
Average B-values ($Å^2$)	117	113	43
Protein	117	113	43
Solvent	0	0	44
Ramachandran favored (%)	98.6	99.0	98.6
Ramachandran allowed (%)	1.4	1.0	1.4

Ramachandran outliers (%)	0	0	0

*Statistics for the highest-resolution shell are shown in parentheses.

[a] $R_{meas} = \frac{\sum_{hkl}[\frac{N(hkl)}{N(hkl)-1}]^{\frac{1}{2}} \times \sum_i |I_i(hkl) - \langle I(hkl)\rangle|}{\sum_{hkl}\sum_i I_i(hkl)}$

[b] $R_{pim} = \frac{\sum_{hkl}\left[\frac{1}{N(hkl)-1}\right]^{\frac{1}{2}} \times \sum_i |I_i(hkl) - \langle I(hkl)\rangle|}{\sum_{hkl}\sum_i I_i(hkl)}$

[c] $CC_{\frac{1}{2}} = \frac{\sum(x-\langle x\rangle)(y-\langle y\rangle)}{[\sum(x-\langle x\rangle)^2 \sum(y-\langle y\rangle)^2]^{\frac{1}{2}}}$

[d] $R_{work} = \frac{\sum||F_{obs}|-|F_{calc}||}{\sum|F_{obs}|}$; R_{free} is defined as R_{work} calculated from 5% of the reflections that were excluded from refinement.